Supplementary material for:

Ribosome provisioning activates a bistable switch coupled to fast exit from stationary phase

P. Remigi, G.C. Ferguson, E. McConnell, S. De Monte, D.W. Rogers and P.B. Rainey

This document contains:
- Supplementary Note
- Supplementary Figures 1-10
- Supplementary Tables 1-4

Supplementary Note:
Model for titration-based molecular switch

We model the intracellular dynamics by means of a set of ordinary differential equations describing the dynamics of the concentration of mRNA produced by a *gene with positive auto-regulation* ($pflu3655$), and whose translation is post-transcriptionally modulated by the competition between ribosomes and a *regulator* (RsmA/E).

The model is inspired by (Mukherji et al. 2011), and its main features, derived from the experimental observations or hypothesized according to standard assumptions on molecular interactions, are illustrated in Fig. 1.

The system is described by three variables that quantify the concentrations of the three components of the mRNA pool: the concentration f of free mRNA, the concentration r of mRNA bound to ribosomes, and the concentration r^* of mRNA bound to the regulator. The level of fluorescence production, as measured using the GFP reporter to the CAP locus, is under the same positive regulation by the gene product as the gene itself. For simplicity, we consider the concentration of proteins encoded by the gene is the same as the mRNA undergoing translation, so that the feedback loop is modelled by the dependence on r of the production of new free mRNA. Similarly, r measures the activation level of the fluorescent reporter/capsulation pathway.

The pools of free ribosomes ρ and of free regulator α interact post-transcriptionally with free mRNA, competing for the same binding site, so that the regulator can sequester a fraction of mRNA, analogous to what happens in other cases of molecular titration.

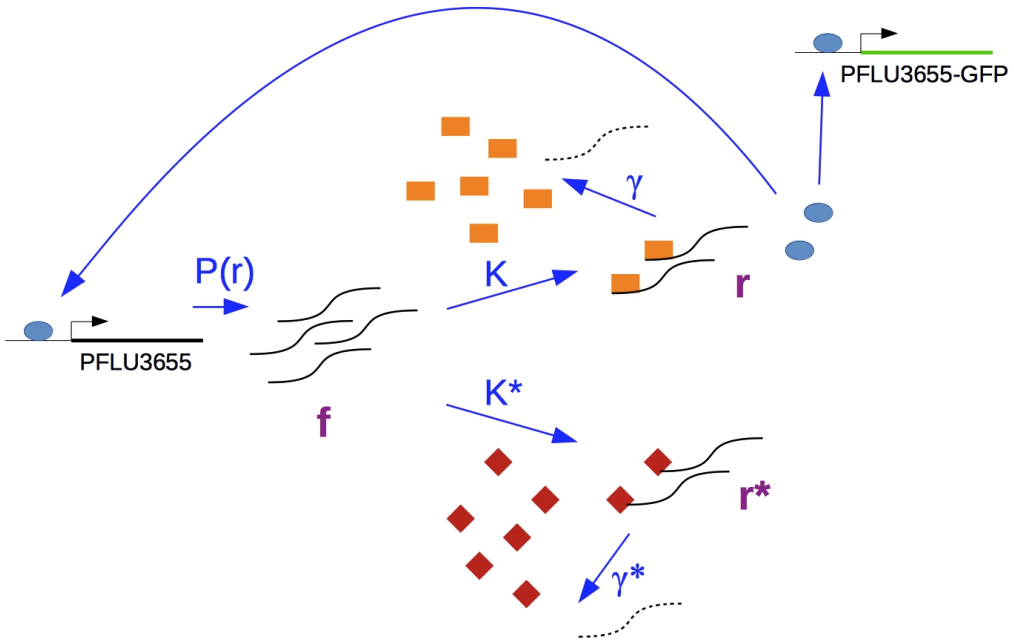

Figure 1: Schematic representation of the hypothesized regulatory pathways, involving competition between ribosomes (orange rectangles) and a regulator (red diamonds) for a target site on the mRNA, activation of the gene transcription by the gene product (blue ellipses), and the GFP reporter construct. The model describes the dynamics of free mRNA concentration f and of that of mRNA bound to either ribosomes (r) or to the regulator (r^*). The rates relative to the transition between these three classes and towards degradation are indicated in blue. The total pool of ribosomes and regulator proteins are assumed to be constant, so that these are either in free form or bound to mRNA.

The equations for the change of the three state variables in time read:

$$\frac{df}{dt} = P(r) - K\rho f - K^*\alpha f \quad (1)$$

$$\frac{dr}{dt} = K\rho f - \gamma r \quad (2)$$

$$\frac{dr^*}{dt} = K^*\alpha f - \gamma^* r^*, \quad (3)$$

where K and K^* are the kinetic constants for binding of mRNA to ribosomes and regulatory molecules, respectively, and γ and γ^* are the decay constants of the two bound mRNA classes (upon which decay, ribosomes and regulators are recycled in the cellular pool). Under the assumption that the pools of ribosomes R and of regulators A change on a slower time scale than the expression of the gene, and if we assume for simplicity that every bound mRNA interacts with a single ribosome/molecule of the regulator, then the pools of free ribosomes ρ and of free regulator α can be computed by subtraction as $\rho = R - r$ and $\alpha = A - r^*$.

The production term $P(r)$ accounts for the positive feedback loop, and is thus assumed to be a positive increasing function with r, saturating at a constant level. For illustration purpose, we will assume that the protein has a binary cooperative binding to the promoter, so that the production rate has the Hill form:

$$P(r) = \frac{a\, r^2}{b + r^2}, \quad (4)$$

but qualitatively similar results hold as well for other functional forms, as discussed later.

Let us now find the equilibrium solutions for eqs. 1-3, which we keep in a general form by expressing the production (source) and binding (sink) terms in the free mRNA equation 1 as functions of the translated mRNA.

From eq. 2, we obtain the equilibrium f as a function of r:

$$f(r) = \frac{\gamma r}{K(R - r)}. \quad (5)$$

By substituting in eq. 3, we obtain the equilibrium r^* as a function of r:

$$r^*(r) = \frac{A}{\frac{c}{g}\frac{R-r}{r} + 1}, \quad (6)$$

where $g = \gamma/\gamma^*$ and $c = K/K^*$.

The equilibrium condition for eq. 1 can now be expressed in terms of r. Let us define as:

$$\begin{aligned} T(r) &= K(R-r)f(r) - K^*\left[A - r^*(r)\right] f(r) = \\ &= \left[1 + \frac{A}{(g-c)\,r + cR}\right]\,\gamma\, r \end{aligned} \tag{7}$$

the term accounting for mRNA binding during post-transcriptional regulation. Since by definition $r < R$, the numerator in eq. 7 is always positive.

$T(r)$ opposes the increase in translation elicited, in the absence of titration, by the positive feedback loop. The equilibria of the system correspond to:

$$P(r) = T(r), \tag{8}$$

that is binding exactly balances production. When $P(r) > T(r)$, then the amount of free mRNA will increase in time, and vice-versa when $P(r) < T(r)$, so that the stability of the equilibria can be assessed by looking at the difference $P(r) - T(r)$ between source and sink terms.

In order to understand the qualitative behaviour of the different strains considered in the main text, we can study graphically the solutions to eq. 8 as the intersections of the two curves $P(r)$ and $T(r)$. For simplicity, we assume that the decay rates are constant and equal, thus $g = 1$. We study the number and position of the equilibria for a set of parameters that corresponds to the qualitative differences among the strains discussed in the main text: ancestral SBW25, the 1B^4 switcher mutant and two genetic constructs with increased PFLU3655 production (1B^4(pME6032-$pflu3655$); see Fig. 3 B from the main text) and decreased binding affinity of the regulator (1B^4 P$_{pflu3655}$G-8A; see Fig. 4 B, C from the main text).

As illustrated in Fig. 2, the two curves always intersect in the origin (as long as the PFLU3655 protein has no other sources of production than the autoregulated $pflu3655$ gene). This trivial equilibrium corresponds to the 'OFF' state, where the gene is not expressed, and cells are not capsulated. If the term $T(r)$ is always larger than the production rate $P(r)$ (Fig. 2 A), then the equilibrium is stable. This case corresponds to regulation in ancestral SBW25 under normal growth conditions, and occurs in a parameter range where the total concentration of regulator A is not too small relative to that of ribosomes R. Even in this situation it is nevertheless possible that, for large stochastic fluctuations, the system remains trapped for a certain time at

high expression levels, due to the fact that the system slows down where the two curves approach, as illustrated by the proximity of the curve $P(r)-T(r)$, to the abscissae axis. This corresponds to the observation of rare, possibly transient, occurrences of capsulation in the SBW25 strain (Gallie *etal*. 2015).

In switcher $1B^4$ strains and ancestral SBW25 in late stationary phase, where ribosome content is high with respect to the regulator, titration is only effective when PFLU3655 production (thus its concentration) is low. When gene transcription exceeds a threshold (the middle, unstable equilibrium), instead, production overcomes post-transcriptional regulation, and amplification caused by the positive feedback loop displaces the system towards a new equilibrium. In such 'ON' equilibrium, the concentration of the transcript is no longer set by the regulator, but rather by other processes that impede the indefinite growth of protein production, such as for instance competition at the promoter binding site of $pflu3655$, which are recapitulated in the saturation of the production term.

If the production term had another functional form, the same type of scenario would occur, provided two conditions are satisfied:

- When $pflu3655$ is expressed at very low levels, production grows slower than titration, so that most mRNA is sequestered by the RsmA/E regulator.

- Protein production saturates for high levels of translation, limiting the autocatalitic effect of the positive feedback loop. For instance, this could be due to exhaustion of tRNAs.

If these conditions are met, then the system will be bistable whenever production outpaces titration for intermediate mRNA concentrations. The transition from a monostable to a bistable scenario corresponds to a (saddle-node) bifurcation occurring when the production curve is tangent to the regulation curve. This happens for parameters that satisfy the following equation, evaluated at the (parameter-dependent) equilibrium points r_E:

$$\frac{\partial P}{\partial r}(r_E) = \frac{\partial T}{\partial r}(r_E) \tag{9}$$

$$= \left\{ 1 + \frac{c\frac{A}{R}}{\left[(g-c)\,\frac{r}{R} + c\right]^2} \right\} \gamma. \tag{10}$$

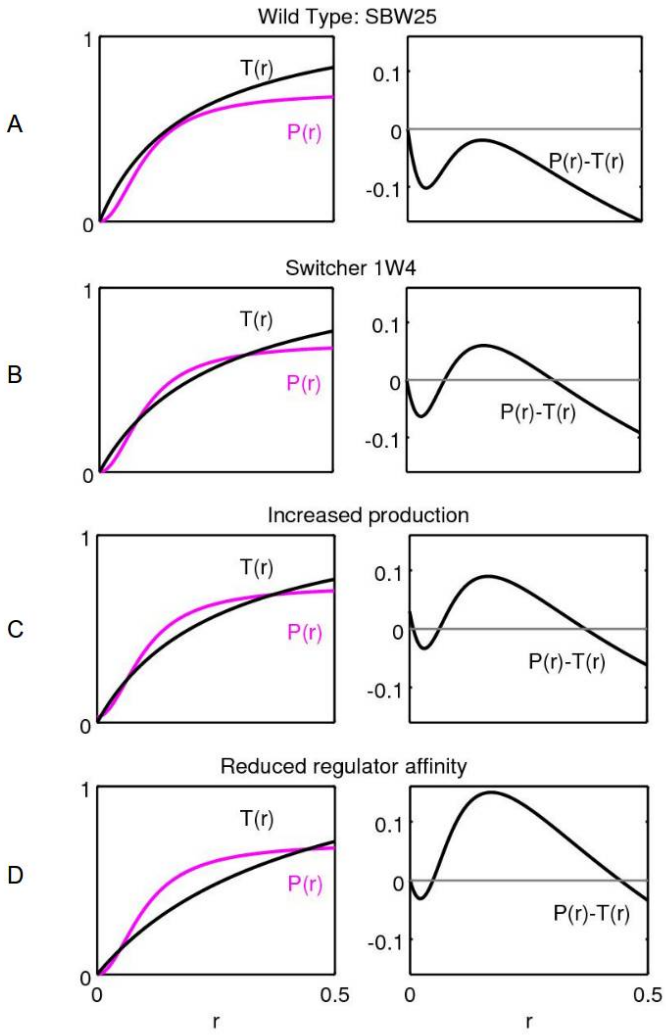

Figure 2: The intersection of the production curve $P(r)$ and of the curve $T(r)$ are the equilibrium points of eqs. 1-3. The figure illustrates the two qualitatively different scenarios that can occur: monostability of the 'OFF' state (A) and three different cases of bistability between 'OFF' and 'ON' states (B-D). Parameter values are: (A) $c = 0.2$, $R = 0.75$; (B) $c = 0.2$, $R = 1$; (C) $c = 0.2$, $R = 1$, but the production term is increased of $\delta = 0.03$; (D) $c = 0.3$, $R = 1$, and $g = 1$, and, in all cases, $\gamma = 0.03$, $A = 30$, $a = 0.7$, $b = 0.01$.

Assuming that regulation of the gene is independent of post-transcriptional processes, thus keeps the same dependence on protein concentration when the interaction between mRNA and ribosomes/regulators is modified, the production term will be described by the same increasing function of r. Since the left-hand side of eq. 9 remains the same, hence, transition to the bistability regime will occur for smaller r when the ratio A/R decreases. At the bifurcation point, the stable and unstable positive equilibria coincide, so that the threshold for the transition to the 'ON' state is smaller for higher levels of ribosomes relative to the regulator.

In the region where three equilibria are present, the position of the middle, unstable equilibrium defines the extension of the basins of attraction of the two stable equilibria 'ON' and 'OFF'. If processes that are not included in this model, such as dynamical changes in other intracellular variables or number fluctuations, cause stochastic variations in the number of proteins produced by the gene $pflu3655$, it is reasonable to think that the relative extension of the basins of attraction quantifies the probability of finding a cell in one of either states, and that the position of the 'ON' equilibrium reflects the level of expression of the CAP locus. We would thus expect that as long as the population is in a steady-state, the phenotypic composition on the population reflects such probabilities.

If the system was instead in a transient state, where the intracellular concentration of ribosomes changes on a time scale comparable to that of the phenotypic switch, this model would not be enough to account for the composition of the population, which is expected to vary due to the coupling of physiological and phenotypic change. Analogously, in order to describe quantitatively the steady state and how it is attained, one would need to model explicitly the effect of stochastic variations.

Let us now consider if this qualitative model is consistent with the experimental observations relative to the genetic constructs in the $1B^4$ background studied in the main article, corresponding in the model to the case illustrated in Fig. 2 B.

One first experiment consisted in overexpressing the gene $pflu3655$. Constitutive expression of $pflu3655$ (under the control of the IPTG-inducible P_{tac} promoter present in the pME6032 plasmid) results in an effective increase in transcription, independent of PFLU3655 protein concentration. We model this by adding to the production term a constant amount. If one substitutes $P(r)$ with $P(r) + \delta$, with $\delta > 1$, the basin of attraction of the 'OFF' equilibrium reduces, thus increasing the probability of switching to the 'ON' state

(Fig. 2 C). At the same time, the production rate in the 'ON' equilibrium is slightly enhanced. This corresponds to an increase both of the proportion of cells in the 'ON' state and of their fluorescence, in agreement with Fig. 3 B from the main text.

In a second experiment, the binding affinity between the mRNA and the regulator was reduced, corresponding to an increase of the parameter c. This variation, illustrated in Fig. 2 D, leads as well to a steep increase of the probability of switching 'ON', as reported in Fig. 4 C of the main text. Concomitantly, the production rate, hence fluorescence, increase, as also observed experimentally (Fig. 4 B, main text).

References

Mukherji S, Ebert MS, Zheng GXY, Tsang JS, Sharp PA, van Oudenaarden A. 2011. MicroRNAs Can Generate Thresholds in Target Gene Expression. Nature Genetics 43: 854–59.

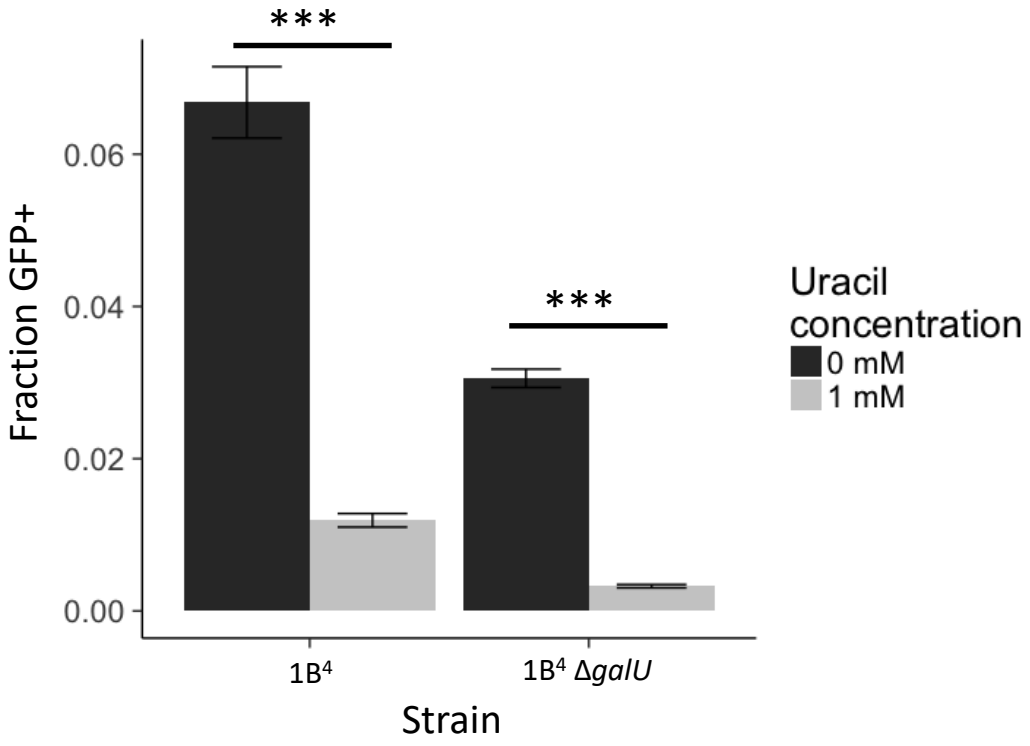

Supplementary Figure 1: Capsulation in the *galU* mutant

The $P_{pflu3655}$-GFP reporter was introduced in $1B^4$ and the *galU* transposon mutant (Gallie *et al.* 2015). Capsulation was measured by quantifying the proportion of GFP positive cells by flow cytometry at the onset of stationary phase. Means ± s.e.m. are shown, n = 12. Data are pooled from 2 independent experiments. *** $P < 0.001$, two-tailed *t*-test.

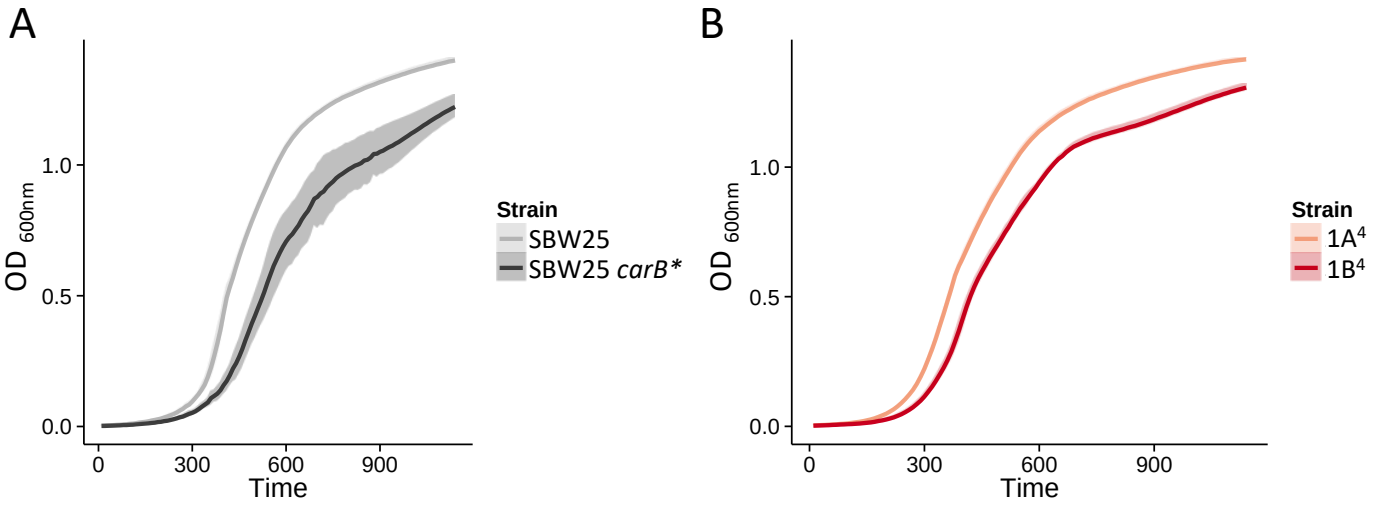

Supplementary Figure 2: Growth rate of *carB* mutants

Growth kinetics of SBW25 and SBW25 *carB** (*A*) or $1A^4$ and $1B^4$ (*B*) strains in KB medium. Lines and shading represent mean ± s.d., respectively, from 4 biological replicates.

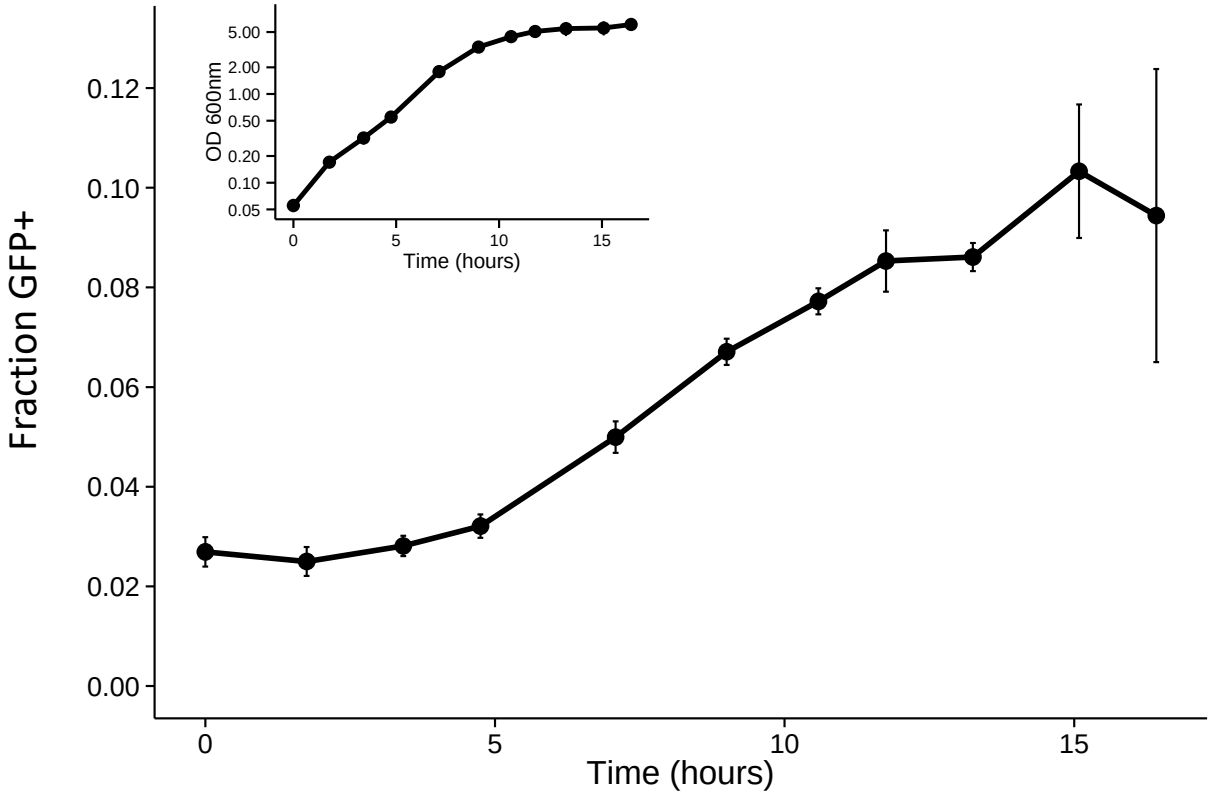

Supplementary Figure 3: Capsulation kinetics in 1B[4]

The $P_{pflu3655}$-GFP reporter was introduced in 1B[4]. OD600nm (inset) and size of GFP positive subpopulation (main panel) were monitored over >15h. Means ± s.d. are shown, n=3. Data are representative of 2 independent experiments.

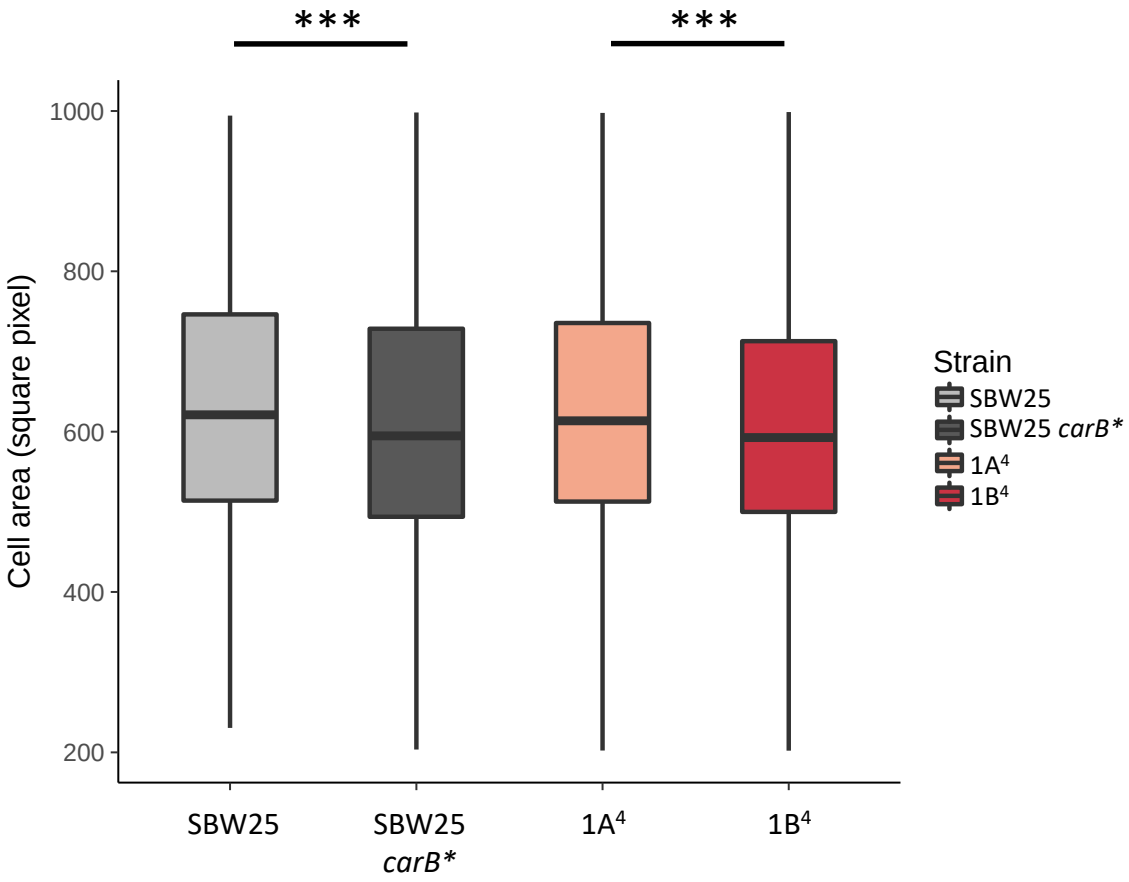

Supplementary Figure 4: The *carB mutation reduces cell size**

Boxplots represent the distribution of cell areas in exponentially growing cultures. n = 1760, 1535, 1420, 1399 for SBW25, SBW25 *carB**, $1A^4$ and $1B^4$, respectively. Data are pooled from 2 independent experiments. *** $P < 0.001$, Wilcoxon test.

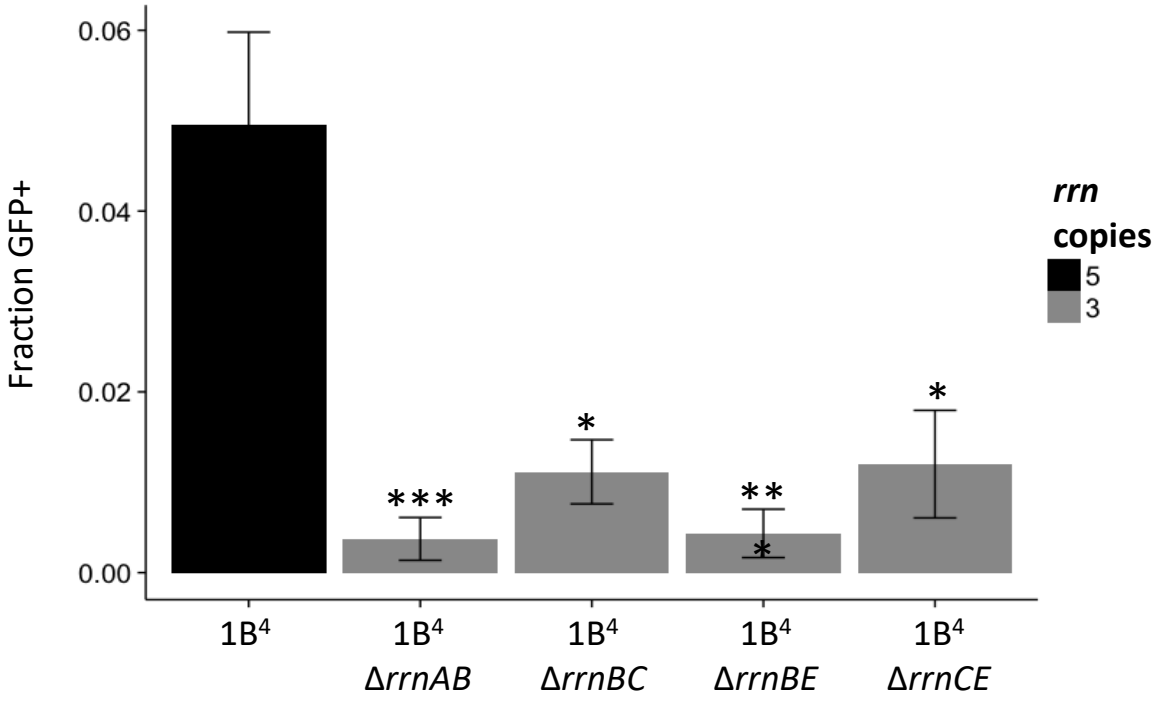

Supplementary Figure 5: Capsulation in double *rrn* mutants

Capsulation was measured by flow cytometry in $1B^4$ and its derived *rrn* double mutants at the onset of stationary phase (OD = 1-2). Means ± s.e.m. are shown. n = 9 ($1B^4$ and $1B^4$ Δ*rrnCE*) or n = 18 (all other strains). Data are pooled from 3 independent experiments. * $P < 0.05$, *** $P < 0.001$, Kruskall-Wallis test with Dunn's post-hoc correction, comparison to $1B^4$.

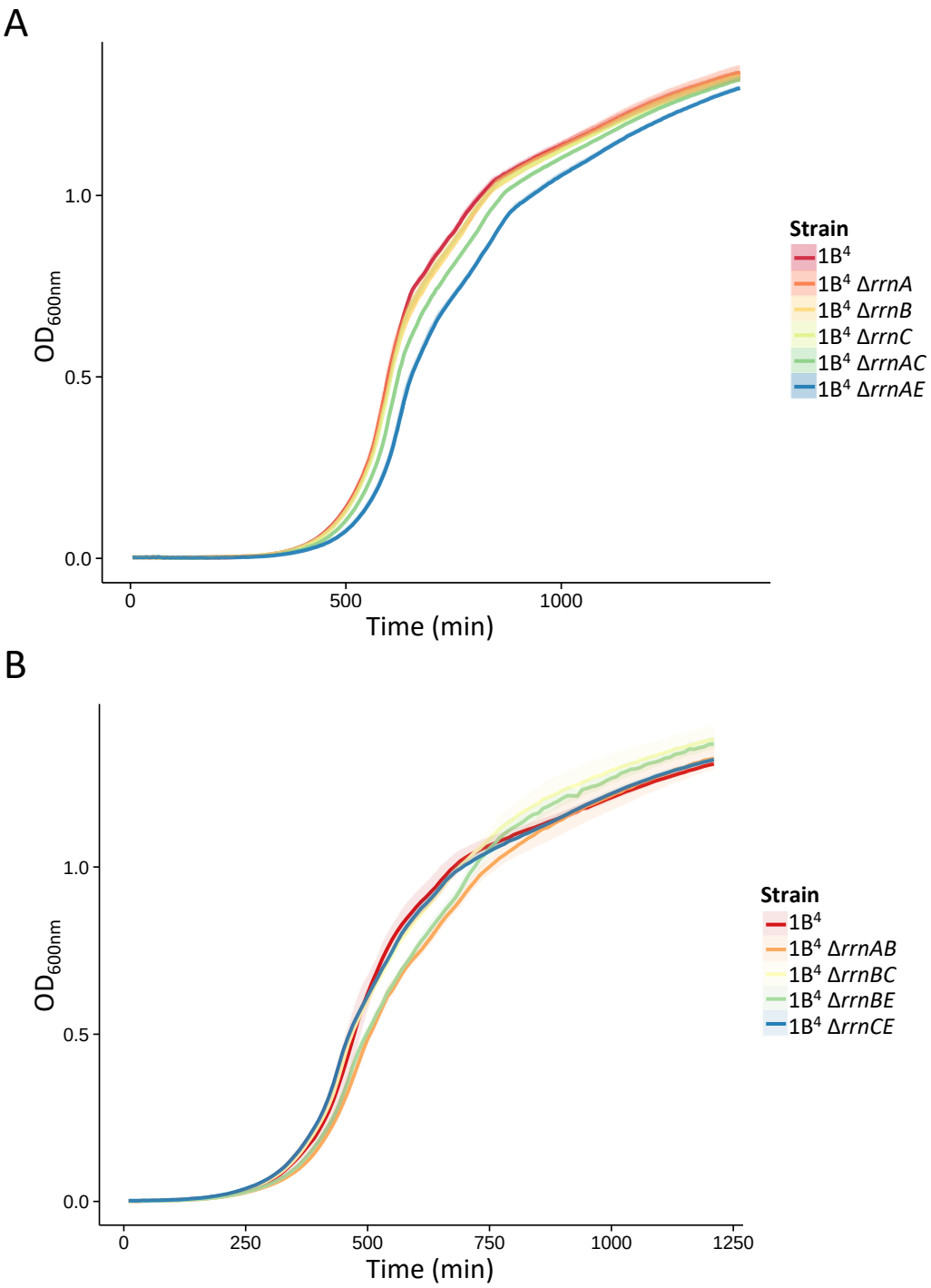

Supplementary Figure 6: Growth rate of *rrn* mutants

Growth kinetics of strain $1B^4$ and its derived double *rrn* mutants in KB medium. Lines and shading represent mean and s.d. from 4 biological replicates, respectively.

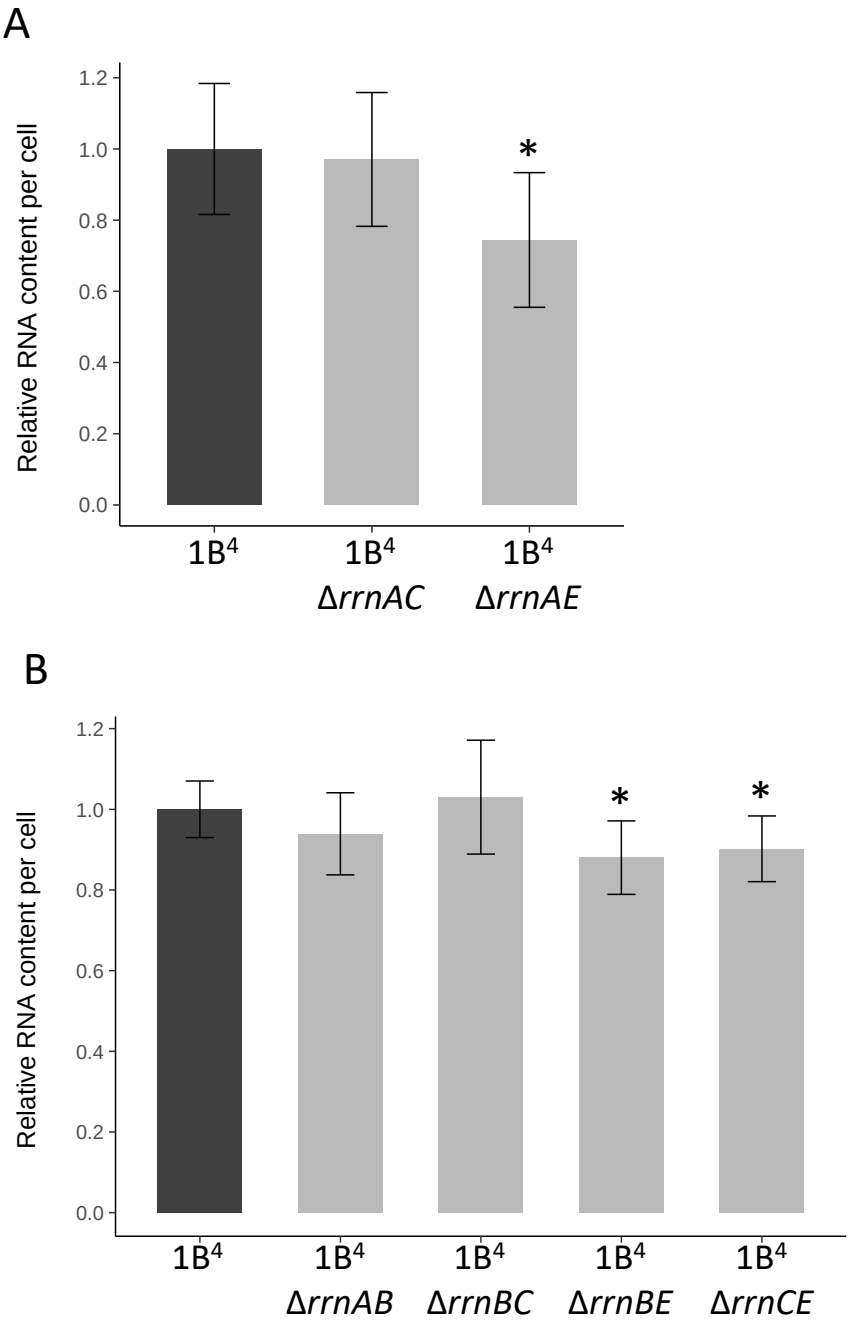

Supplementary Figure 7: RNA quantification in *rrn* mutants

Total RNA content in bacterial cells during exponential phase (OD = 0.5-0.6) normalized per cell count. Values were normalized to SBW25 or 1B^4 controls within each experiment. Means ± s.d. are shown, n=6 (*A*) or n=8 (*B*). * $P < 0.05$, two-tailed *t*-test compared to 1B4 values.

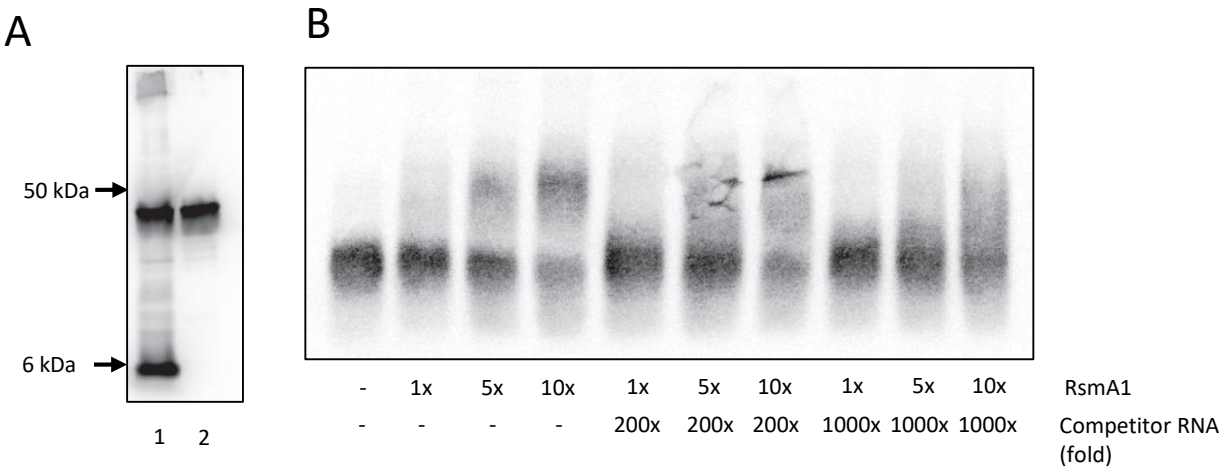

Supplementary Figure 8: Control experiments for electrophoretic mobility shift assays
(*A*) Anti-His_6 western-blot of samples obtained after anti-His_6 purification of total proteins extracted from SBW25(pME6032-His_6-*rsmA1*) (line 1) or SBW25(pME6032-*rsmA1*) cultures (line 2). His_6RsmA1 is detected as a 6kDa band. Non-specific binding of the anti-His_6 antibody to a ~50kDa protein indicates equal loading of the two samples.
(*B*) RsmA1 binding to *pflu3655* mRNA is decreased by the addition of unlabelled competitor RNA. EMSA experiments were performed with 6.25nM biotin labelled oligonucleotides corresponding to the wild-type *pflu3655* sequence and increasing concentrations of purified His6-RsmA1. Unlabelled competitor RNA was added to a ratio of 200x or 1000x.

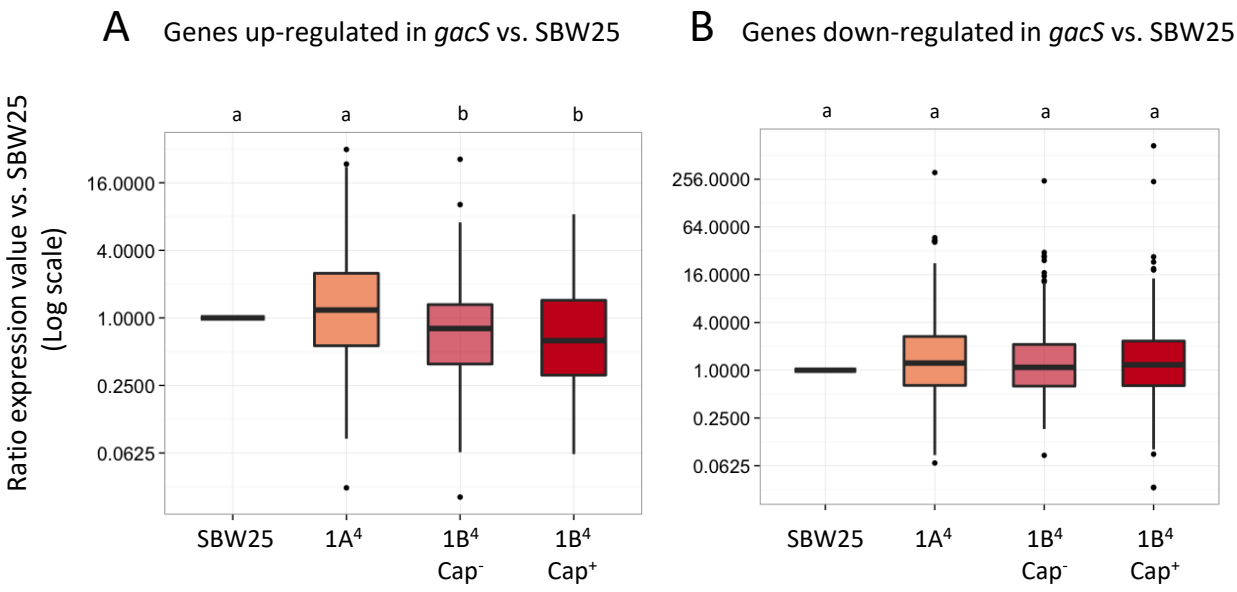

Supplementary Figure 9: Expression of *gacS*-regulated genes

Genes that are up-regulated (left) or down-regulated (right) more than 4 times in a *gacS* mutant compared to wild-type SBW25 were recovered from Cheng *et al.* (2013). The distribution of induction or repression values (after normalisation by the base expression in SBW25) in the different RNA-seq datasets is shown for each set of genes. n = 125 (*A*) or n = 165 (*B*). Letter groups indicate statistical significance, $P < 0.05$, Kruskall-Wallis test with Dunn's post-hoc correction.

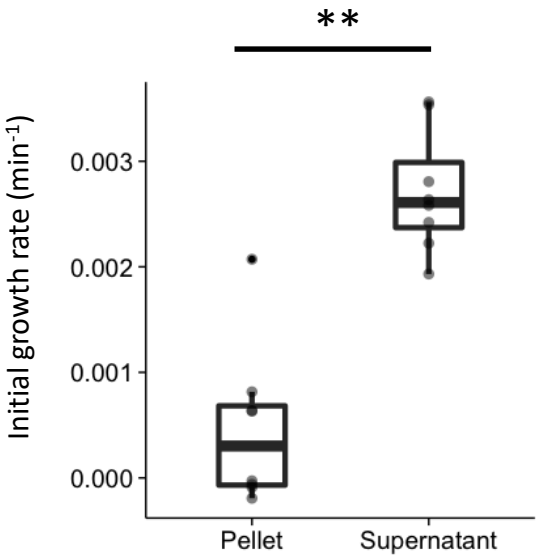

Supplementary Figure 10: Growth rate of SBW25 cultures enriched in Cap⁻ or Cap⁺ cells
Cells from 7 day-old colonies were resuspended in fresh KB and suspensions were enriched in Cap⁻or Cap⁺cells. Growth of these suspensions in 96-well plates was monitored for 2h. n = 8. Data are pooled from 2 independent experiments. ** *P* = 0.0078, Wilcoxon test.

SBW25 vs. 1A^4									
KEGG pathway enriched in SBW25 vs. 1A^4	Term size	Genes in term	*P*	adj. *P*	KEGG pathway enriched in 1A^4 vs. SBW25	Term size	Genes in term	*P*	adj. *P*
00430 Taurine and hypotaurine metabolism	9	4	0,043779	1	00643 Styrene degradation	15	7	0,011899	0,586534
00480 Glutathione metabolism	26	8	0,047884	1	03009 Ribosome biogenesis	64	19	0,020136	0,586534
00051 Fructose and mannose metabolism	21	6	0,111106	1	02040 Flagellar assembly	36	12	0,02456	0,586534
04122 Sulfur relay system	17	5	0,127528	1	02060 Phosphotransferase system (PTS)	7	4	0,025612	0,586534
00562 Inositol phosphate metabolism	13	4	0,146475	1	00550 Peptidoglycan biosynthesis	25	9	0,029925	0,586534
01220 Degradation of aromatic compounds	28	7	0,155986	1	00072 Synthesis and degradation of ketone bodies	11	5	0,037458	0,611807
00130 Ubiquinone and other terpenoid-quinone biosynthesis	14	4	0,180185	1	00561 Glycerolipid metabolism	15	6	0,043957	0,615398
00564 Glycerophospholipid metabolism	24	6	0,181877	1	00261 Monobactam biosynthesis	12	5	0,054652	0,651227
00680 Methane metabolism	25	6	0,208693	1	00650 Butanoate metabolism	41	12	0,063741	0,651227
00450 Selenocompound metabolism	10	3	0,212169	1	00903 Limonene and pinene degradation	9	4	0,067545	0,651227

1A^4 vs. 1B^4 Cap$^-$									
KEGG pathway enriched in 1A^4 vs. 1B^4 Cap$^-$	Term size	Genes in term	*P*	adj. *P*	KEGG pathway enriched in 1B^4 Cap$^-$ vs. 1A^4	Term size	Genes in term	*P*	adj. *P*
00643 Styrene degradation	15	9	0,000179	0,017498	02040 Flagellar assembly	36	17	1,7E-05	0,00169
00364 Fluorobenzoate degradation	5	4	0,003281	0,160767	00280 Valine, leucine and isoleucine degradation	45	15	0,004404	0,215789
00627 Aminobenzoate degradation	18	8	0,005145	0,168059	Carbon metabolism	137	33	0,014162	0,433112
00561 Glycerolipid metabolism	15	6	0,026766	0,655755	00071 Fatty acid degradation	35	11	0,021939	0,433112
00380 Tryptophan metabolism	34	10	0,044427	0,738479	00072 Synthesis and degradation of ketone bodies	11	5	0,023823	0,433112
00362 Benzoate degradation	26	8	0,054049	0,738479	00281 Geraniol degradation	15	6	0,026517	0,433112
03030 DNA replication	31	9	0,059387	0,738479	00630 Glyoxylate and dicarboxylate metabolism	56	15	0,035325	0,49455
00040 Pentose and glucuronate interconversions	14	5	0,067819	0,738479	00430 Taurine and hypotaurine metabolism	9	4	0,046997	0,540975
00053 Ascorbate and aldarate metabolism	14	5	0,067819	0,738479	00640 Propanoate metabolism	44	12	0,049681	0,540975
01501 beta-Lactam resistance	30	8	0,111262	1	00440 Phosphonate and phosphinate metabolism	10	4	0,068322	0,557962

$1A^4$ vs. $1B^4$ Cap^+									
KEGG pathway enriched in $1A^4$ vs. $1B^4$ Cap^+	Term size	Genes in term	*P*	adj. *P*	KEGG pathway enriched in $1B^4$ Cap^+ vs. $1A^4$	Term size	Genes in term	*P*	adj. *P*
02030 Bacterial chemotaxis	70	27	0,000477	0,046757	03010 Ribosome	54	32	7,6E-11	7,4E-09
00643 Styrene degradation	15	9	0,00105	0,051432	02040 Flagellar assembly	36	21	2,2E-07	1,1E-05
00364 Fluorobenzoate degradation	5	4	0,007797	0,231816	00910 Nitrogen metabolism	22	9	0,015346	0,501301
01503 Cationic antimicrobial peptide (CAMP) resistance	29	12	0,009462	0,231816	00760 Nicotinate and nicotinamide metabolism	26	8	0,108702	1
00627 Aminobenzoate degradation	18	8	0,020407	0,39997	00290 Valine, leucine and isoleucine biosynthesis	18	6	0,113597	1
00380 Tryptophan metabolism	34	12	0,036062	0,58901	00253 Tetracycline biosynthesis	7	3	0,134295	1
00040 Pentose and glucuronate interconversions	14	6	0,052016	0,59648	00220 Arginine biosynthesis	36	10	0,136746	1
00053 Ascorbate and aldarate metabolism	14	6	0,052016	0,59648	00460 Cyanoamino acid metabolism	11	4	0,143509	1
00471 D-Glutamine and D-glutamate metabolism	5	3	0,06429	0,59648	03009 Ribosome biogenesis	64	16	0,15226	1
00361 Chlorocyclohexane and chlorobenzene degradation	5	3	0,06429	0,59648	Carbon metabolism	137	31	0,176931	1

$1B^4$ Cap^- vs. $1B^4$ Cap^+									
KEGG pathway enriched in $1B^4$ Cap^- vs. $1B^4$ Cap^+	Term size	Genes in term	*P*	adj. *P*	KEGG pathway enriched in $1B^4$ Cap^+ vs. $1B^4$ Cap^-	Term size	Genes in term	*P*	adj. *P*
02030 Bacterial chemotaxis	70	29	1,3E-06	0,000131	00564 Glycerophospholipid metabolism	24	6	0,144571	1
00630 Glyoxylate and dicarboxylate metabolism	56	19	0,001725	0,074061	00770 Pantothenate and CoA biosynthesis	19	5	0,149217	1
00362 Benzoate degradation	26	11	0,002267	0,074061	00550 Peptidoglycan biosynthesis	25	6	0,167299	1
00072 Synthesis and degradation of ketone bodies	11	6	0,005318	0,117082	00364 Fluorobenzoate degradation	5	2	0,167821	1
00340 Histidine metabolism	26	10	0,007977	0,117082	00561 Glycerolipid metabolism	15	4	0,182305	1
00380 Tryptophan metabolism	34	12	0,00835	0,117082	00643 Styrene degradation	15	4	0,182305	1
02020 Two-component system	196	47	0,008363	0,117082	00730 Thiamine metabolism	10	3	0,184028	1
00430 Taurine and hypotaurine metabolism	9	5	0,010112	0,123873	00910 Nitrogen metabolism	22	5	0,232943	1
00900 Terpenoid backbone biosynthesis	16	7	0,011716	0,127571	03060 Protein export	17	4	0,250724	1
01501 beta-Lactam resistance	30	10	0,023554	0,212244	00627 Aminobenzoate degradation	18	4	0,286739	1

Supplementary Table 1: Top 10 KEGG pathways whose genes are enriched in the different RNAseq comparisons.

Over-represented pathways with an adjusted P value < 0.05 are highlighted in green.

Strain	Reference
P. fluorescens	
SBW25	Zhang *et al.* 2006
SBW25 *lacZ*	Zhang & Rainey 2007
SBW25 *carB**	Beaumont *et al.* 2009
1A4	Beaumont *et al.* 2009
1B4	Beaumont *et al.* 2009
1B4 Tn5-*galU*	Gallie *et al.* 2015
1B4 Δ*rrnA*	This work
1B4 Δ*rrnB*	This work
1B4 Δ*rrnC*	This work
1B4 Δ*rrnE*	This work
1B4 Δ*rrnAC*	This work
1B4 Δ*rrnAE*	This work
1B4 Δ*rrnBC*	This work
1B4 Δ*rrnBE*	This work
1B4 Δ*rrnCE*	This work
1B4 Δ*pflu3655*	This work
1B4 ΔgacA	This work
1B4 Δ*rsmA1*	This work
1B4 Δ*rsmE*	This work
SBW25 P*pflu3655* G-8A	This work
SBW25 P*pflu3655* GG-7AC	This work
SBW25 P*pflu3655* A33T	This work
1B4 P*pflu3655* G-8A	This work
1B4 P*pflu3655* GG-7A	This work
1B4 P*pflu3655* A33T	This work

Supplementary Table 2: Bacterial strains used in this study

Name	Purpose	Description	Sequence
oPR156	Deletion *rrn* operons	*rrnB/C/E* overlap fwd	AAAACCCCATGAGAGGATCGAAACGTTAATAGAGC
oPR157		*rrnB/C/E* overlap rev	CGTTTCGATCCTCTCATGGGGTTTTGTTTTGGGCG
oPR158		*rrnB* up fwd	CAGTACTAGTCTTGTGGCCTGGATATGGGG
oPR159		*rrnB* down rev	CAGTACTAGTGGTACAAATCAGAATGCCTGCAT
oPR160		*rrnC* up fwd	CAGTACTAGTATATAGAATGTAGAGCGCCCAG
oPR161		*rrnC* down rev	CAGTACTAGTCCGTCCTACGTAACCGATCG
oPR164		*rrnE* down rev	CAGTACTAGTACCTGCTGATGGGGCGT
oPR165		*rrnE* up fwd	CAGTACTAGTGTCCATTGCTGATCCACCTCG
oPR166		*rrnA* up fwd	CAGTACTAGTAATTATCTGACGACAGGTGCCTC
oPR167		*rrnA* overlap rev	TGCCGCATCTGAGAGGATCGAAACGTTAATAGAGC
oPR168		*rrnA* overlap fwd	TTCGATCCTCTCAGATGCGGCAGTTGATAGATCC
oPR169		*rrnA* down rev	CAGTACTAGTCTACAGCTTGCTTGTACCAAGGA
oPR170	Site-directed mutagenesis of *pflu3655* promoter	P*pflu3655* GG-7AC fwd	GCCTTGCATGCCGGAAAAGACAGTAGGTGATGCATTTTTC
oPR171		P*pflu3655* GG-7AC rev	GAAAAATGCATCACCTACTGTCTTTTCCGGCATGCAAGGC
oPR174		P*pflu3655* G-8A fwd	GCATCACCTACTCCTTTTTCCGGCATGCAAGGC
oPR175		P*pflu3655* G-8A rev	GCCTTGCATGCCGGAAAAAGGAGTAGGTGATGC
oPR176		P*pflu3655* A33T fwd	CTTTACGCATAGTCCGAGCAATAGCGAGGACGT
oPR177		P*pflu3655* A33T rev	ACGTCCTCGCTATTGCTCGGACTATGCGTAAAG
oPR37	Deletion of *pflu3655*	*pflu3655* up fwd; SpeI	CAGTACTAGTCGTTTCTCGACAGCCTGGTG
oPR212		*pflu3655* overlap rev	CTCGCTATTCACCTACTCCCTTTTCCGGCATGC
oPR213		*pflu3655* overlap fwd	GAAAAGGGAGTAGGTGAATAGCGAGAAAATCCCCC
oPR214		*pflu3655* down rev; SpeI	TGACACTAGTATTGGGGGTGAAGTCGTGCA
oPR206	Complementation/over-expression of *pflu3655*	*pflu3655* fwd; EcoRI	GATCGAATTCGTGATGCATTTTTCCAACGTCCT
oPR207		*pflu3655* rev; XhoI	GATCCTCGAGCTATTCACGATTCGACCGCTCC
oPR223	Reverse oligo to amplify *pflu3655* region (with oPR37)	*pflu3655* rev; SpeI	TGACACTAGTCTGCCTGACAATGTTGAAGTCA
oPR91	Deletion of *rsmA1*	*rsmA1* up fwd; SpeI	TCAGACTAGTTCAATCAGTCAATTCATGATTGGTAAA
oPR92		rsmA1 overlap rev	GTGAGGAGAAAGGTATGGAACCAAGCCTTTAATTTTTATCGTT
oPR93		*rsmA1* overlap fwd	AATTAAAGGCTTGGTTCCATACCTTTCTCCTCACGCAT
oPR94		*rsmA1* down rev; SpeI	TCAGACTAGTCAGCCTCGGTTCAAAGGTGT
oPR97	Deletion of *rsmE*	*rsmE* up fwd; SpeI	TCAGACTAGTAGACCGTGGCGTGTGTGAT
oPR98		*rsmE* overlap rev	GCTACTGAGGGGGCTATGTTTCAGACAGGGCAGGT
oPR99		*rsmE* overlap fwd	CCCTGTCTGAAACATAGCCCCCTCAGTAGCCAG
oPR100		*rsmE* down rev; SpeI	TCAGACTAGTCGCAATTACCGGAATCGTGC
oPR148	P*rrnB* -GFP reporter	P*rrnB* up fwd; SpeI	CAGTACTAGTTATGCATCTATAGGTGCGCTGC
oPR151		P*rrnB* -GFP overlap rev	TCCTCTTTAATCTTCAGTTCAAACATCTTTGGGTT
oPR152		P*rrnB* -GFP overlap fwd	TGAACTGAAGATTAAAGAGGAGAAATTAAGCATGCG
FluomarkerP2		*gfp* 3.1-T0 down rev	AATCTAGAGGATTCTCACCAATAAAAAACG
oPR244	RT-qPCR	*rpsL* fwd	TAACTCGGCACTGCGTAAAGTA
oPR245		*rpsL* rev	TGACCTTCACCACCGATGTAC
oPR236		*gyrA* fwd	GCGGTAAAGGTAAATCGGCT
oPR237		*gyrA rev*	TTGCCCTTGCTGGAGAACA
oPR69	Cloning of His_6-*rsmA1*	*rsmA1* fwd	GATCCTCGAGTTAAAGGCTTGGTTCTTCGTCC
oPR70		*rsmA1* rev	GATCGAATTCATGCTGATTCTGACTCGTCGT
DRW037		site-directed mutagenesis His_6 tag	CACAGGAAACAGAATTCATGCATCACCATCACCATCACATGCTGATTCTGACTCGTCGT
DRW038		site-directed mutagenesis His_6 tag	GAATTCTGTTTCCTGTGTGAAATTGTTATCCGCTCACA
DRW100	*In vitro* transcription	P*pflu3655* amplification fwd	TAATACGACTCACTATAGGGATGCCGGAAAAGGGAGTAGG
DRW101		P*pflu3655* amplification rev	TTCGATTGAGTCCGTGCA

Supplementary Table 3: Oligonucleotides used in this study

Plasmids	Description	Reference or source
pRK2013	Helper plasmid, Tra^+ Kan^R	Ditta *et al.* 1980
pUX-BF13	Helper plasmid for transposition of the Tn7 element, Amp^R	Bao *et al.* 1991
pUC18R6K-mini-Tn7T-Gm	A Tn7-based integration vector, Gen^R	Choi *et al.* 2005
pUC18R6K-mini-Tn7T-Gm-P*pflu3655* -GFP	Cloning of the promoter of *pflu3655* fused to *gfpmut3* into pUC18R6K-mini-Tn7T-Gm, Gen^R	Gallie *et al.* 2015
pUC18R6K-mini-Tn7T-Gm-P*pflu365* 5-GFP G-8A	Introduction of the G-8A mutation by site directed mutagenesis into pUC18R6K-mini-Tn7T-GmPpflu3655-GFP, Gen^R	This work
pUC18R6K-mini-Tn7T-Gm-P*pflu365* 5-GFP GG-7AC	Introduction of the GG-7AC mutation by site directed mutagenesis into pUC18R6K-mini-Tn7T-GmPpflu3655-GFP, Gen^R	This work
pUC18R6K-mini-Tn7T-Gm-P*pflu365* 5-GFP A33T	Introduction of the A33T mutation by site directed mutagenesis into pUC18R6K-mini-Tn7T-GmPpflu3655-GFP, Gen^R	This work
pUC18R6K-miniTn7-P*rrnB* -GFP	Cloning of the promoter of *rrnB* fused to *gfpmut3* into pUC18R6K-mini-Tn7T-Gm, Gen^R	This work
pME6032	Shuttle vector for gene expression in Pseudomonas, Tet^R	Heeb *et al.* 2002
pME6032-*pflu3655*	pME6032 containing the *pflu3655* gene, Tet^R	This work
pME6032-*rsmA1*	pME6032 containing the *rsmA1* gene, Tet^R	This work
pME6032-His_6-*rsmA1*	pME6032 containing the His_6-*rsmA1* gene, Tet^R	This work
pUIC3	Integration vector with promoterless '*lacZ* , Mob^+ Tet^R	Rainey 1999
pUIC3-Δ*rrnA*	Construct for *rrnA* deletion cloned into pUIC3, Tet^R	This work
pUIC3-Δ*rrnB*	Construct for *rrnB* deletion cloned into pUIC3, Tet^R	This work
pUIC3-Δ*rrnC*	Construct for *rrnC* deletion cloned into pUIC3, Tet^R	This work
pUIC3-Δ*rrnE*	Construct for *rrnE* deletion cloned into pUIC3, Tet^R	This work
pUIC3-Δ*pflu3655*	Construct for *pflu3655* deletion cloned into pUIC3, Tet^R	This work
pUIC3-P*pflu3655* G-8A	G-8A site-directed mutagenesis in P*pflu3655* for re-introduction in SBW25 genome, Tet^R	This work
pUIC3-P*pflu3655* GG-7AC	GG-7AC site-directed mutagenesis in P*pflu3655* for re-introduction in SBW25 genome, Tet^R	This work
pUIC3-P*pflu3655 A33T*	A33T site-directed mutagenesis in P*pflu3655* for re-introduction in SBW25 genome, Tet^R	This work
pUIC3-Δ*gacA*	Construct for *gacA* deletion cloned into pUIC3, Tet^R	XX. Zhang
pUIC3-Δ*rsmA1*	Construct for *rsmA1* deletion cloned into pUIC3, Tet^R	This work
pUIC3-Δ*rsmE*	Construct for *rsmE* deletion cloned into pUIC3, Tet^R	This work

Supplementary Table 4: Plasmids used in this study